Intermolecular Anionic Mixed-Valence and π-Dimer Complexes of *Ortho*-Pentannulated BisAzaCoroneneDiimides

Arthur H. G. David,[a] Maxime Roger,[a] Olivier Alévêque,[a] Heorhii Melnychenko,[a] Laura Le Bras,*[b] Magali Allain,[a] Adèle Gapin,[a] David Canevet,[a] Olivier Ségut,[a] Eric Levillain,*[a] and Antoine Goujon*[a]

[a] A. H. G. David, M. Roger, O. Alévêque, H. Melnychenko, M. Allain, A. Gapin, D. Canevet, O. Ségut, E. Levillain,* A Goujon*
MOLTECH-Anjou, SFR MATRIX
Univ Angers, CNRS
2 Bd Lavoisier, 49000 Angers, France
E-mail: eric.levillain@univ-angers.fr, antoine.goujon@univ-angers.fr

[b] L. Le Bras*
Chrono-environnement, CNRS
Université de Franche-Comté
16 route de Gray, 25030 Besançon, France
E-mail: laura.le_bras@univ-fcomte.fr

This study reports the serendipitous discovery of intermolecular anionic mixed-valence (MV) and π-dimer species in *ortho*-pentannulated BisAzaCoroneneDiimides (BACDs) during their electrochemical reduction in a non-aqueous solvent. A library of nitrogen-containing extended PDIs was synthesized *via* an aza-benzannulation reaction followed by a Pd-catalysed *ortho*-pentannulation reaction. *Ortho*-pentannulated BACDs revealed strong aggregation abilities in solution. Concentration-dependent UV-vis absorption spectra, variable temperature ^{1}H NMR experiments, and atomic force microscopy coupled to molecular dynamics support their self-assembly into columnar aggregates. Cyclic voltammetry experiments in dichloromethane reveal prominent splitting of the first reduction wave, attributed to the formation of unprecedented intermolecular anionic MV and π-dimers in organic solvent. These species were thoroughly characterized by real-time spectroelectrochemistry, electrochemical simulations and theoretical calculations. Remarkably, this work underscores the tuneable nature of AzaBenzannulatedPerylene Diimides (AzaBPDIs) and BACDs, emphasizing their potential as a promising scaffold for designing supramolecular materials with long-range radical anion delocalization. The observation of this phenomenon provides insights into the fundamental behaviour of supramolecular organic semiconductors, thereby paving the way for the development of novel electronic devices and electron-deficient materials.

Introduction

The challenging self-assembly of highly electronically conductive materials from small molecules showing strong intermolecular electronic communication is a highly promising perspective for the bottom-up fabrication of electronic devices and the development of supramolecular electronics.[1,2] The corresponding materials present undeniable advantages such as self-healing or stimuli-responsiveness.[3,4] However, the lack of direct covalent π-conjugations between electroactive units or redox active centres limits their ability to conduct charges with high efficiencies. The incorporation of Mixed-Valence (MV) species or states in such materials has been employed to enhance their performances.[5,6] MV species consist of molecules where two redox centres (RC) at different oxidation states communicate through a bridge (B). The charge is shared to varying degrees between the two sites leading to two extreme cases: in negatively charged species, such molecules can be described as $RC^{n-} - B - RC^{(n-1)-}$ if the electron is mostly localized on one RC, or as $RC^{(n-0.5)-} - B - RC^{(n-0.5)-}$ if the electron is fully delocalized across both sites.[7] The electronic coupling between the two sites leads to intervalence charge transfer (IVCT),[8] resulting in characteristic absorption bands at low energy. Although the most well-known MV species are Creutz-Taube bis-ruthenium complexes and analogous organometallic species,[9–11] fully organic architectures can also exhibit this behaviour[6,12,13] upon reduction or oxidation and are particularly interesting in the development of high-performance organic semiconductors. Indeed, the potential of MV-based (semi)conductors lies in their ability to generate materials where electrons or holes can freely flow over long distances with very high mobilities.[6,14] Organic MV phenomena have been commonly observed in positively charged tetrathiafulvalene (TTF)[15–18] or bipyridinium[19] crystals as example. Organic compounds capable of affording anionic MV species are however scarcer and are mostly represented by quinone or (di)imide derivatives. In most cases, MV states emerge as an intramolecular phenomenon, where redox centres communicate through a π-conjugated bridge, even though through-space interactions in flexible dimers[20] also afforded IVCT signatures and MV states. While MV states have been observed in highly pre-organized crystals,[21,22] polymer films,[23] discrete coordination cages,[24] mechanically interlocked molecules[25–27] or hydrogen-bonded supramolecular xerogels,[28] or dendrimers,[29] reports of spontaneous self-assembly of intermolecular MV complexes in organic solvents from two discrete molecules are extremely rare.[30] Moreover, intra and intermolecular MV states have been vastly over-represented by cationic species. In that regard, the characterization of anionic MV states, even more so intermolecular examples, remains elusive. Recent studies from Seo, Baik, Byon and co-workers revealed that naphthalene diimides (NDIs) decorated with cationic side-groups formed weak MV dimers $[NDI\text{-}NDI]^{\cdot-}$ upon electrochemical reduction of 0.5 equiv. e^- per NDI,[31] echoing seminal reports from Miller.[23,32,33] Their analysis is based on the appearance of an IVCT band in the near-infrared (NIR) region, a response in electronic paramagnetic resonance and the slight broadening of the first reduction wave seen in cyclic voltammetry (CV). This unusual result was achieved using a concentrated

aqueous KCl solution as solvent, which considerably enforces a strong ionic strength and hydrophobic effect, significantly enhancing intermolecular NDI π-π stacking. Even under such highly favourable conditions, the broadening without clear splitting of the first reduction event in CV tends to indicate a weak comproportionation constant K_{com}, *i.e.* a weakly coupled and associated MV complex. Furthermore, Wasielewski, Stoddart, Li and co-workers detected in 2019 a moderate splitting in a broadened first reduction wave of a NDI derivative in water,[34] indicating the formation of a MV state in conditions where the hydrophobic effect prevails. Olivier and co-workers observed the appearance of broad absorption bands in the NIR that could be attributed to IVCT by chemical and electrochemical reduction of NDIs[35] and perylene diimides (PDIs)[36] stacks. Nonetheless, here again as in the previous examples, the driving force for the formation of weakly associated MV species is the strong hydrophobic effect. The absence of large splitting is the sign that in these example, MV and π-Dimer states coexist in equilibrium. Thus, to the best of our knowledge, the spontaneous and selective self-assembly of anionic intermolecular MV species in competitive or dissociative organic solvents, where the formation of a strongly associated MV dimer is the driving force, has not been observed and characterized in depth. This missing point in these fundamental undergoing investigations may come from the fact that electron-deficient organic semiconductors are lagging far behind their electron-rich counterparts in terms of both diversity and performances, underscoring the necessity of designing new electron-poor
conjugated molecules to unlock novel properties andreactivities.[37,38] Herein, we report the synthesis and self-assembly of *ortho*-pentannulated BisAzaCoroneneDiimides (BACDs) and AzaBenzannulatedPerylene Diimides (AzaBPDIs), which spontaneously generate strongly associated anionic intermolecular MV species upon electrochemical reduction in organic medium (**Figure 1**). The observation and characterization of this anionic intermolecular MV state is supported by a combination of cyclic voltammetry and spectroelectrochemistry

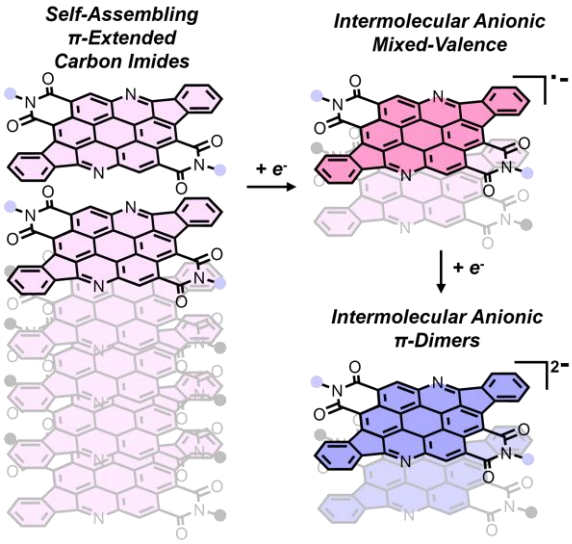

Figure 1. Self-assembling *ortho*-pentannulated BACDs affording intermolecular MV and π-dimers in solution after electrochemical reduction.

experiments coupled with mathematical modelling and quantum chemistry calculations. The clear and large splitting of the first reduction wave observed in CV experiments, still visible around 10 µM concentration range for the BACDs, demonstrates remarkably strong intermolecular non-covalent bonding interactions in the MV supramolecular complexes. It also demonstrates that by progressive electron injection, MV and π-Dimer states can be selectively reached. By comparing the electrochemical properties of ten extended rylene diimide dyes, we were able to identify the critical structural and electronic parameters required for these molecules to form MV species upon partial reduction. This emergence of organic intermolecular anionic MV in organic solvents, discovered serendipitously, is an original observation and remarkable result. Considering the strong potential and relevance of rylene diimides and analogous dyes as n-type organic semiconductors, we believe that this study paves the way toward the construction of self-assembled highly conductive n-type supramolecular MV materials of high interest in organic and supramolecular electronics.

Results and Discussion

Synthesis and X-ray Structures

A library of nitrogen-containing extended PDIs (**Figure 2a**) bearing either ethylpropyl (for AzaBPDIs) or 2-octyldodecyl (for BACDs) imide chains were prepared *via* a light-driven azabenzannulation reaction[39] between amine-decorated PDIs and 2-bromobenzaldehyde derivatives. This was followed by a Pd-catalysed intramolecular C−H arylation[40,41] in the *ortho* position of the PDI, affording five-membered rings and fused electron-deficient π-surfaces. The use of functionalized 2-bromobenzaldehydes allowed for the introduction of methoxy electron-donating groups or electron-withdrawing trifluoromethyl groups. Branched 2-octyldodecyl groups for the *ortho*-pentannulated BACDs were selected to ensure good solubility in common organic solvents. Mono-annulated AzaBenzannulatedPerylene Diimides (AzaBPDIs) were prepared from NH_2PDI while bis-annulated BACDs were synthesized from regiopure 1,6-$(NH_2)_2$PDI and 1,7-$(NH_2)_2$PDI *via* our recently reported route.[42] Reactions of NH_2PDI with 2-bromobenzaldehyde derivatives in acidic medium, followed by light irradiation in a white-light photoreactor and oxidation with 2,3-dichloro-5,6-dicyano-1,4-benzoquinone (DDQ) afforded intermediates **Br-aPDIs** in excellent yields (76-88%, **Scheme S1**). Subsequently, a screening of the reaction conditions (**Table S1**) for the Pd-catalysed pentannulation reaction of intermediates **Br-aPDIs** was performed. The best reaction conditions were found with $Pd(dba)_2$ (10%) as catalyst, SPhos (20 %) as ligand, and DBU (2 equiv.) as base carrying out the reaction in NMP at 160 °C under microwave (MW) irradiation for 2 h and yielding compound **aPDI-Ph** in an excellent 83% yield (see **Scheme S2,S3**).[43] These optimized conditions were successfully used for the synthesis of *ortho*-pentannulated AzaBPDIs (**Scheme S3**) **aPDI-OMe** (55% yield) and **aPDI-CF_3** (71% yield). This synthetic strategy was applied to the synthesis of *ortho*-pentannulated BACDs **1,6-Ph**, **1,6-OMe**, **1,6-CF_3**, **1,7-Ph**, **1,7-OMe**, **1,7-CF_3**. The double azabenzannulation reactions with 2-bromobenzaldehyde derivatives on 1,6-$(NH_2)_2$PDI and 1,7-$(NH_2)_2$PDI gave compounds **1,7-BACDs** and **1,6-BACDs** in good

yields (71-84%) while Pd-catalysed pentannulation reactions afforded the targeted extended BACDs in moderate yields (25-54%, see **Schemes S4,S5,S6**). Single crystals of fused AzaBPDIs **aPDI-Ph** (**Figures 2b,S187**) and **aPDI-CF₃** (**Figures 2c,S188**) were grown by slow evaporation of Et_2O in $CHCl_3$ solution of the compounds. Both fused AzaBPDIs display a flat and rigid aromatic system. Their packing revealed the formation of columnar structures formed by alternating dimers on account of their π-π interactions. **aPDI-Ph** exhibits dimers with a donor-acceptor stack where the fused phenyl side-group of one molecule faces the electron deficient perylene diimide core of the other, while **aPDI-CF₃** presents dimers with a rotated face-to-face stack where the electron deficient perylene diimide cores faces each other. Single crystals of intermediate **Br-aPDI-Ph** (**Figure S186**) were grown by slow evaporation of Et_2O in CH_2Cl_2 solution of **Br-aPDI-Ph**. This X-ray crystal structure shows that the AzaBPDI core of intermediate **Br-aPDI-Ph** is flat and possesses a twisted peripheral phenyl ring due to the bromine atom in its *ortho* position. Again, the packing of **Br-aPDI-Ph** exhibits columnar structures where the electron deficient perylene diimide cores face each other. These arrangements highlight the ability of such molecules to aggregate by π-π interactions on account of their extended aromatic system.

Aggregation in Solution

All *ortho*-pentannulated BACDs show signs of strong aggregation in solution when analysed by variable temperature (VT) ^{1}H NMR spectroscopy. **1,6-Ph** and **1,7-Ph** displayed broad aromatic peaks at 25 °C in $CDCl_3$ which were sharpening and deshielding when increasing the temperature to 55 °C (**Figures S103,S111**). Again, in $C_2D_2Cl_4$, broad aromatic peaks could be observed at 25 °C while well-defined aromatic peaks were obtained by heating the sample above 100 °C (**Figure 3a** and **Figures S105,S106,S113,S114**). The chemical shifts kept evolving and deshielding until 120 °C, hinting at reminiscent intermolecular non-covalent interactions even at high temperature. A similar behaviour was observed for **1,6-CF₃** and **1,7-CF₃** (**Figures S123,S124,S132,S133**). The methoxy-decorated molecules were more complex to study, as no peak was visible at 25 °C no matter which deuterated solvent was tested (**Figures S142,S147**). Heating up the samples at 120 °C in $C_2D_2Cl_4$ allowed for the measurement of a defined spectrum for **1,6-OMe** (**Figures S139,S140,S141**) while **1,7-OMe** remained challenging to characterize (**Figure S148**). These observations suggest a robust π-π stacking in solution on account of strong non-covalent bonding interactions, as it can be expected for such large rylene derivatives. In contrast, the *ortho*-pentannulated AzaPDIs did not show aggregation properties as strong as their *ortho*-pentannulated BACDs counterparts. Further investigations on the aggregation of the *ortho*-pentannulated BACDs were performed by UV-vis absorption spectroscopy. Compared to their parent AzaPDIs,[39] the **aPDI-Ph** and **aPDI-CF₃** dyes show a red shifted absorption (**Figures S1,S5**). Noticeably, they feature a much more complex vibronic structure between 400 and 550 nm, and a sharper band at high energy, centred on 380 nm for **aPDI-Ph** and

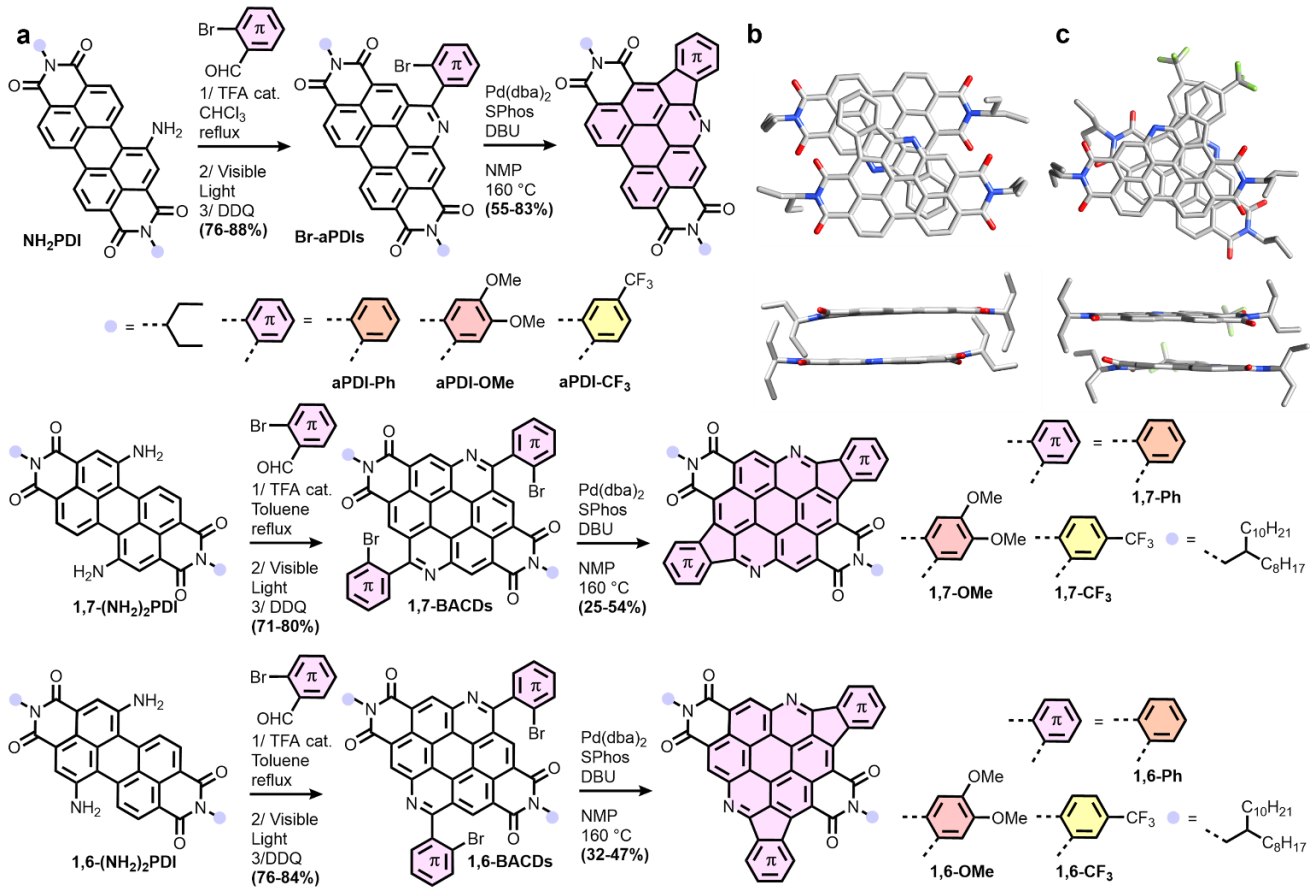

Figure 2. a) Synthesis and structures of *ortho*-pentannulated AzaBPDIs and BACDs studied in this work. Top-down and side-on views of the π-stack dimers formed by b) **aPDI-Ph** and c) **aPDI-CF₃** in their single-crystal X-ray structure. Hydrogen atoms and solvent molecules are omitted for the sake of clarity. Colour coding: C, grey; O, red; N, blue; F, green.

378 nm for **aPDI-CF$_3$**. **aPDI-OMe** exhibits sharps absorption peaks between 350 and 500 nm and a broad, weaker band from 500 up to 650 nm attributed to an intramolecular charge-transfer (**Figure S9**). Both **aPDI-Ph** and **aPDI-CF$_3$** exhibit moderate emissive properties between 500 and 700 nm (**Figures S4,S8**) with fluorescence quantum yields (Φ_f) reaching 14 and 20 % respectively in $CHCl_3$, while **aPDI-OMe** is not photoluminescent. At low concentration, *ca.* 1×10^{-6} M bis-annulated **1,6-Ph** and **1,7-Ph** display a slight red-shift of their sharp band accompanied by a loss of hyperfine structure between 400 and 550 nm (**Figures S12,S18**) compared to their *ortho*-pentannulated AzaPDIs counterparts. The main absorption band of the 1,6 regioisomers are broader and slightly red-shifted compared to their 1,7 analogues. The same trend is observed for **1,6-CF$_3$** and **1,7-CF$_3$** (**Figures S24,S30**). For dyes **1,6-OMe** and **1,7-OMe** a broadening of all peaks is observed along with an enlargement of the charge-transfer band reaching *ca.* 750/800 nm (**Figures S36,S41**). Although the *ortho*-pentannulated BACDs possessing peripheral methoxy groups are non-luminescent, the BACDs bearing naked fused phenyl rings or peripheral trifluoromethyl groups display fluorescence properties (**Figures S17,S23,S29,S35**) in the same spectral region compared to their

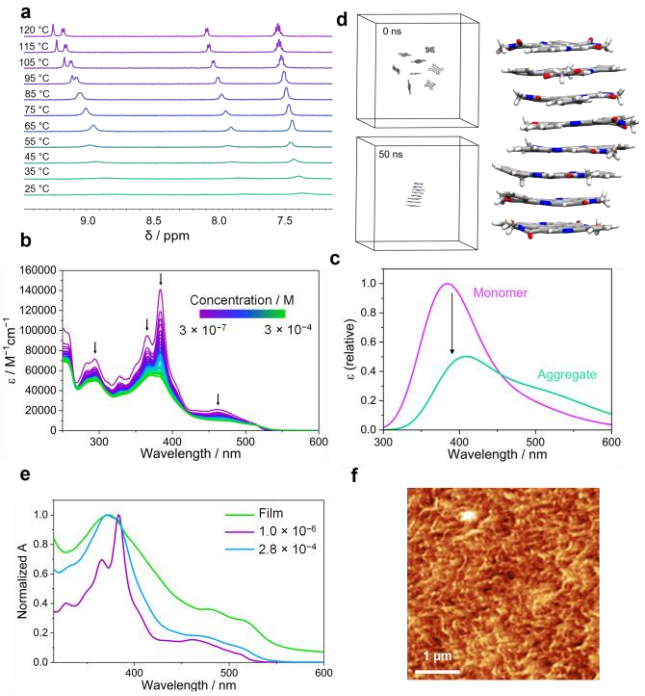

Figure 3. Self-assembly behaviour of **1,7-Ph**. a) VT ^{1}H NMR (500 MHz) from 25 to 120 °C in $C_2D_2Cl_4$ (*ca* 2 mM) showing the progressive disassembly of supramolecular aggregates originated from π-π stacking. ε is the apparent molar absorption coefficient (A / C_{total} × l). b) Concentration-dependant absorption spectra in $CHCl_3$. c) Calculated absorption spectra for the monomer and a model dimer showing the broadening of the spectrum upon aggregation along with a decrease of ε. d) Representation of the simulation box containing eight **1,7-Ph** before (top) and after (bottom) 50 ns simulation. The final columnar aggregate is also represented. For the sake of clarity, the solvent molecules (CH_2Cl_2) have not been represented within the simulation box. e) Normalized absorption spectra at low-concentration (purple line), high concentration (blue line) and in thin film (green line) showing significant changes in absorption upon aggregation. f) AFM image of the thin film in tapping mode.

extended AzaBPDIs analogues. However, their Φ_f is lower, reaching only 8% for **1,7-CF$_3$** (**Table S2**). The evolution of their optical properties at different concentrations, between *ca.* 3×10^{-7} and 5×10^{-4} M, in $CHCl_3$ was investigated and confirmed the ability of the *ortho*-pentannulated BACDs to aggregate in organic chlorinated solvents (**Figure 3b and Figures S12,S18,S24,S30,S36,S41**). *Ortho*-pentannulated BACDs exhibited a significant alteration of their absorption spectra when increasing the concentration: a progressive loss of vibronic structure and a decrease of the calculated apparent molar absorption coefficient ε (A / C_{total} × l), suggesting the self-association of molecules into supramolecular assemblies of lesser ε. These changes were drastic at low concentrations, but their intensity weakened above concentrations around 10^{-4} M for most compounds and a plateau was reached when plotting apparent ε versus concentration. The evolution of the UV-vis absorption spectra of these *ortho*-pentannulated BACDs versus concentration was used to study the self-association of these compounds. Out of several self-association models, the isodesmic one fitted best the plot of the fraction of aggregated molecules (α_{agg}) versus concentration for all six *ortho*-pentannulated BACDs (see discussion in the SI for the fitting and **Figures S14,S20,S26,S32,S38,S43**). The self-association constants K_a were determined by a nonlinear least-squares fitting method (**Table S3**). This study revealed that, in $CHCl_3$ solution, *ortho*-pentannulated BACDs are strongly self-assembling into supramolecular polymers with K_a in the range of 10^5. In contrast, mono-annulated *ortho*-pentannulated AzaBPDIs did not exhibit this behaviour. Although slight changes in the ε apparent values were detected for all three compounds, no loss of vibronic structure was observed, and the data obtained for those compounds did not fit any self-association models. Thin-films of the *ortho*-pentannulated BACDs were obtained by spin-coating $CHCl_3$ solutions on glass substrates. All extended BACDs showed a drastic broadening and loss of fine structures (**Figures S16,S22,S28,S34,S40,S45**), a sign of strong intermolecular interactions between the aromatic core of the dyes in the solid state. Interestingly, the UV-vis absorption spectra recorded in $CHCl_3$ solution at high concentrations (10^{-4} M) and in thin films are similar (**Figure 3e**), supporting the fact that these molecules are strongly aggregated in solution at these concentrations. These observations were corroborated by atomic force microscopy (AFM) imaging in tapping mode, which revealed a long-range fibrillar organisation in the film (**Figure 3f**). To gain insight into the morphologies of the aggregates formed in solution, molecular dynamics simulations (see description in SI) were performed on a model compound **1,7-Ph** with methyl groups as imide chains to reduce calculation time (**Figure 3d**). A stable columnar stacking was quickly observed over the first 10 ns of the 50 ns simulation. It is worth noticing that no disaggregation process has been observed despite the dynamic character of the assembly. Different stacking patterns have been characterized (**Figure S82**), all corresponding to face-to-face H-type aggregates. The predominant one presents a tilt of 30 ° between the two planes of the molecules. The intermolecular mean distance of 3.5 Å is constant, independently of the stacking motif. Optical properties of both isolated (monomer, M) and aggregated molecules (dimer, D) have also been calculated and are in line with experimental observations (**Figures 3c and S83**), confirming that the origin of the concentration-dependence of the UV-vis absorption spectra of the *ortho*-pentannulated BACDs is their self-

assembly (**Table S5**). A global decrease of the oscillator strength *f* (proportional to ε) for supramolecular species was calculated, *f* being equal to 0.99 and 0.51 for λ_{max} of M and D respectively. The representation of the molecular orbitals of the main absorption band of the dimer reveals a delocalization of the electron density on both molecules. The slight experimental-theoretical mismatch can be attributed to the fact that various stacking patterns (in proportion and in structure) contribute to the global spectrum and are not considered here. In conclusion, the six *ortho*-pentannulated BACDs reported in this study can strongly self-assemble into columnar supramolecular polymers in chlorinated solvents, however, rendering their characterization difficult.

Electrochemistry

To investigate the electronic properties of these materials, CVs were performed in CH_2Cl_2 (0.1 M $TBAPF_6$, 100 mV/s, 10^{-4} M ferrocene calibration) at various concentrations. Typical rylene diimide dyes display two reversible reduction waves,[44,45] corresponding to the successive generation of the anion radical $M^{\cdot-}$ and dianion M^{2-} species. Measurements on extended BACDs revealed a distinct splitting of the first reduction event. The magnitude of the splitting directly correlates with the dye's structure: bis-annulated, fully fused systems exhibited significant splitting regardless of concentration, whereas mono-annulated derivatives displayed weak splitting or broadening, disappearing upon dilution (**Figure 4**). Upon reduction of *ortho*-pentannulated BACDs at 10^{-3} M, a strong splitting of the first reduction wave was observed for all studied molecules. This splitting was corroborated by deconvolution of the cyclic voltammograms, revealing two distinct events in the first reduction wave. The largest splitting was observed for **1,6-CF₃** with 0.30 V (**Figure S61**), and clearly persisted even at concentrations as low as 1 × 10^{-5} M for all five fused BACDs studied (**Figure S55,S58,S61,S64,S67**). Furthermore, all redox events observed during these experiments were fully reversible. In the case of mono-annulated *ortho*-pentannulated AzaBPDIs, compounds **aPDI-Ph** (**Figure 4**) and **aPDI-OMe** (**Figure S52**) revealed a more typical CV albeit with a slight broadening of the first event, possibly indicating a similar but less pronounced behaviour. Interestingly, mono-annulated derivative **aPDI-CF₃** (**Figure 4**) revealed a stronger broadening, possibly attributed to a splitting of the first reduction event, more visible by deconvolution of the CV. This splitting nearly disappeared upon sample dilution, underscoring the intermolecular and supramolecular nature of the observed phenomenon. With the aim of understanding the structure-property relationship between these extended PDIs and the splitting event, control molecules were synthesized (see the detailed synthetic procedures in the SI, **Schemes S7,S8**). **C-CF₃**, *ortho*-pentannulated AzaBPDI analogue of **aPDI-CF₃** equipped with longer 2-octyldodecyl chains, exhibited a weak splitting event at 10^{-3} M, which, this time, persisted upon dilution to 5 × 10^{-5} M (**Figure S73**), unlike **aPDI-CF₃**. In addition, **C-1,6**, non-fused 1,6 regioisomer BACD analogue of **1,6-Ph**, also displayed a splitting but of smaller amplitude compared to **1,6-Ph** and its fully fused systems (**Figure S70**). These experiments show that the appearance of this splitting and its strength depend on both geometrical and electronic features of the dyes. These events were reinforced for (i) the most rigid compounds possessing the largest π-surfaces, and (ii) compounds bearing long chains improving lateral van der Waals interactions. Furthermore, this splitting is more pronounced in molecules bearing electron-withdrawing side-groups. To propose a preliminary hypothesis fitting these observations, we can refer to previously reported systems that exhibited such splitting, albeit almost exclusively observed in the positive direction during the first oxidation step. This behaviour was detected in electron-rich TTF-based derivatives where the redox centres are pre-organized face-to-face along a polymer,[16] in a tweezer,[20] or dendrimers.[29] This concentration-dependent electrochemical behaviour has been explained by a square scheme mechanism,[30] where two redox couples coexist within a narrow potential window: $TTF^{\cdot+}$/TTF and $\pi D^{2+}/MV^{\cdot+}$, referring to intermolecular cationic mixed valence dimer $MV^{\cdot+}$ and cationic π-dimer πD^{2+}, respectively. To the best of our knowledge, the direct observation and characterization of intermolecular anionic mixed valence $MV^{\cdot-}$ and anionic π-dimer πD^{2-} species in organic solvents have not yet been reported. NDIs[35] and PDIs[36] displaying significant broadening events of the first reduction wave were detected in water, where extremely powerful hydrophobic interactions prevail, generating strong self-assembled systems. In organic solvents, these inter-chromophores electronic interactions have been observed only when precisely covalently organized[46] or stacked in cyclophanes,[47–50] tweezers,[51] and mechanically interlocked molecules.[25] Thus, the strong and reversible splitting of the first reduction wave, observed during these CV experiments performed in non-aqueous solvents, i.e. CH_2Cl_2, when employing

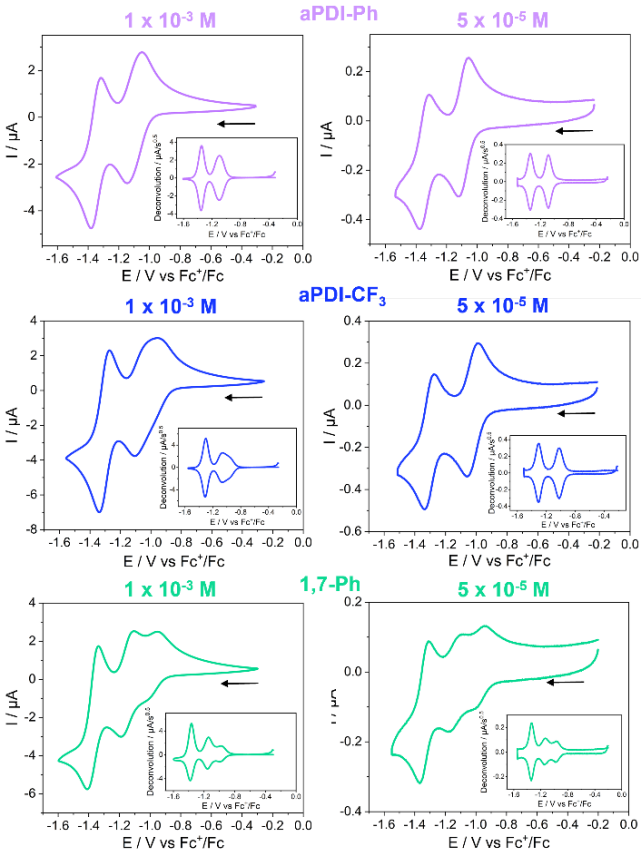

Figure 4. Cyclic voltammetry experiments performed in CH_2Cl_2 (0.1 M $TBAPF_6$, 100 mV/s, 10^{-4} M ferrocene calibration) at high (left, 1 × 10^{-3} M) and low (right, 1 × 10^{-5} M) concentrations for **aPDI-Ph** (purple line), **aPDI-CF₃** (blue line) and **1,7-Ph** (green line) with their deconvoluted data as inserts.

ortho-pentannulated BACDs, is remarkable due to its purely intermolecular nature in the absence of spatial pre-organisation.

Spectroelectrochemistry

To investigate the nature and properties of the species generated during the splitting event, spectroelectrochemical experiments[52–54] were conducted on **1,7-Ph**. Cyclic voltammetry experiments under thin-layer (TLCV) conditions (thickness < 25 µm and scan rate ≤ 10 mV/s) were coupled with spectrophotometric measurements to monitor in real-time (i.e., 1 optical spectrum per mV applied) the variation of spectroscopic signatures in the UV-visible and near-infrared (NIR) regions of the electro-generated anionic forms of *ortho*-pentannulated BACDs (**Figure 5**). With a noticeable splitting, several optical events occur in the NIR range (see **Figure S80** for UV-visible range) when applying potential in the negative direction (**Figure 5a**). As TLCV experiment starts, the neutral form (M) persists and consequently, no new absorption band appeared in the NIR range, resulting in a zero optical signal in this range until the applied potential becomes sufficiently negative to reduce M and induce changes in the absorption bands. Indeed, M does not initially absorb in the NIR window. Subsequently, three events emerge successively: two during the first splitted reduction step and one during the second reduction step (**Figure 5b and c**), associated with absorptions in the 900-1300 nm range. This is characteristic of IVCT bands observed in MV species and the NIR absorption of π-dimers complexes.[31–33,35,36] These signatures can be studied in more detail using Principal Component Analysis (PCA) to mathematically extract the principal component (PC) of each event (**Figure 5b/f**). The first two optical events can be explained by the formation of the radical anion $M^{\bullet-}$, associated with an intermolecular mixed valence dimer ($MV^{\bullet-}$, PC 1), and a fully reduced π-dimer (πD^{2-}, PC 2). The last event is linked to the formation of the dianion M^{2-} (PC 3, around 900 nm). The identification of each species is supported by quantum mechanics calculations (*vide infra*). The proposed square scheme mechanism is displayed in **Figure 5e**. The reduction of M leads to the formation of the radical anion $M^{\bullet-}$, instantly associating with M, to form an intermolecular mixed valence dimer $MV^{\bullet-}$ (*via* K_{MV}). $MV^{\bullet-}$

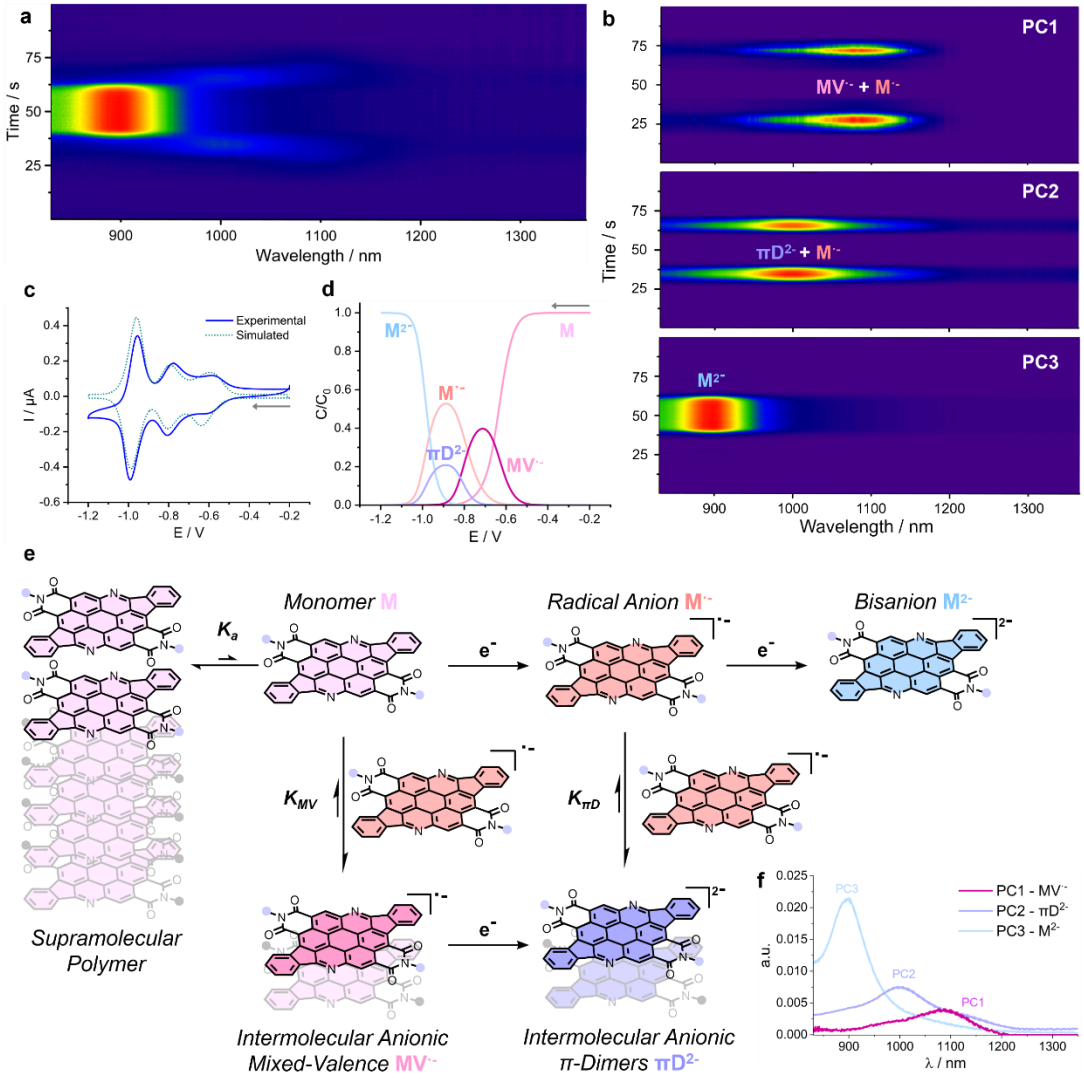

Figure 5. Spectroelectrochemical experiments for **1,7-Ph**. a) Absorption map in function of time during spectroelectrochemistry experiments. b) Extracted principal components of the optical response of each three electrochemical events observed in CVs. c) Thin-layer CVs (0.1 M $TBAPF_6$, 10 mV/s) and simulated CV. d) Simulated concentration profile of each species during CV experiments. e) Associated square scheme mechanism. f) Plotted optical spectra of each PC.

is then reduced to πD^{2-}, a species in equilibrium with $M^{\bullet-}$ (*via* $K_{\pi D}$). These two events explain the splitting observed in CV experiments in solution (**Figure 4**) and in thin-layer conditions (**Figure 5c**). Two distinct optical signatures can be extracted during this phenomenon (**Figure 5b/f**). The formation of $M^{\bullet-}$ and $MV^{\bullet-}$ is associated with a broad absorption band in the NIR from around 900 to 1200 nm with a shoulder centred at 1095 nm. Then, the formation of πD^{2-} alongside the formation of $M^{\bullet-}$ afford another broad NIR absorption band, absorbing up to 1200 nm but this time with a maximum at 1000 nm. The signature of $M^{\bullet-}$, concomitantly formed by reduction of M throughout the splitting process overlaps those of $MV^{\bullet-}$ and πD^{2-}. The complete electrochemical process, the mechanism involving a square scheme and the interpretation of electrochemical and spectroelecrochemical data were validated by simulations using DigiElech 8 and KISSA-1D softwares[55] (see SI for details). Simulated CVs successfully reproduced the splitting events (**Figure 5c**) and the concentration dependence (**Figure S76**). Moreover, the associated simulated concentration profiles (**Figure 5d**) derived from simulated CVs validated the spectroelectrochemical data. The successive observation of intermolecular mixed-valence $MV^{\bullet-}$ and π-dimer πD^{2-} optical signatures alongside the radical anion signature explained the optical response obtained for each event of the splitting. At last, it confirmed that the significant splitting observed in our system is linked to the formation of strong and stable intermolecular mixed valence $MV^{\bullet-}$. Indeed, the amplitude of the splitting is linked to $K_{MV}/K_{\pi D}$: it is more significant when K_{MV} significantly largely exceeds $K_{\pi D}$ (**Figure 5e** and **Figure S76**), thus leading to a large ΔE, the difference between the two maximums of the splitting event of the first reduction wave. This fact and the concentration profile (**Figure 5d**) reveal an important property of this system: by progressive electron injection, $MV^{\bullet-}$ states can be selectively formed, without co-existence with πD^{2-}. This differentiates *ortho*-pentannulated BACDs from previously reported rylene imides aggregated in aqueous medium. Indeed, the weak or absence of clear splitting in CV experiments in these examples reveals that all events happen in a very narrow potential window, thus all species co-exist at the same time.[31,34,36] The same experiments were performed on **1,6-Ph**, exhibiting a similar trend, red-shifted to slightly higher wavelength (**Figures S77,S78,S79**).

Molecular Modelling and Quantum Chemistry Calculation

Structural, energetic, and optical properties of monomer and dimer species as neutral (M and D), anion radical ($M^{\bullet-}$ and $MV^{\bullet-}$) and dianion forms (M^{2-} and πD^{2-}) have been investigated through quantum mechanics calculations[56] (see description in SI). The successive reduction processes impact the structure of the dimer. The average intermolecular distance within the dimer is equal to 3.95, 3.75, and 3.70 Å for D, $MV^{\bullet-}$, and πD^{2-} respectively, highlighting a tighter packing for reduced dimeric species. The relative energies of all the species have been computed to confirm the mechanism of the square scheme (**Table S6** and **Figure S85**). The neutral monomer M being the energy reference, $M^{\bullet-}$ and M^{2-} are more stable with Gibbs free energies (ΔG) of -266 and -249 kJ·mol^{-1} respectively. Their dimer equivalents are more stable to a lesser extent with ΔG ranging from -14 kJ·mol^{-1} for D and -142 kJ·mol^{-1} for πD^{2-}. After the initial reduction of the monomer, the formation of $MV^{\bullet-}$ is the most favoured event (Δ(ΔG) = -113 kJ·mol^{-1}) compared to the formation of M^{2-}(Δ(ΔG) = +17 kJ·mol^{-1}). Once $MV^{\bullet-}$ is reached, its reduction is energetically favoured (Δ(ΔG) = -29 kJ·mol^{-1}) as the dissociation of πD^{2-} (Δ(ΔG) = -107 kJ·mol^{-1}). Furthermore, the optoelectronic properties of anion radical and dianion have been computed. Interestingly, the radical anion in $M^{\bullet-}$ is delocalized over the whole conjugated system (**Figure S84**). From the calculation of their UV-Vis absorption properties (**Figure 6**), we can confirm the trend observed in the NIR range during spectroelectrochemistry experiments. Calculated λ_{max} for the main transitions are localized at 1273, 1190, 1058, and 905 nm for $MV^{\bullet-}$, $M^{\bullet-}$, πD^{2-}, and M^{2-} respectively. Despite the reproduction of the trend of variation of the optical properties upon reduction observed in spectroelectrochemistry, there is a mismatch between the calculated and experimental λ. This comes from experimental parameters not taken in account during calculations, such as the presence of the electrolyte, the concentration and once again the different stacking patterns. The anionic dimers $MV^{\bullet-}$, and πD^{2-} exhibit lower *f* (and thus ε)

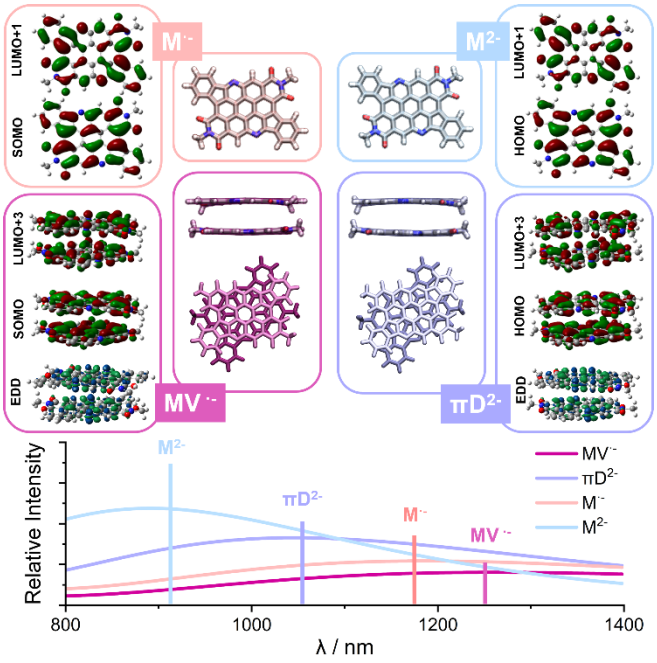

Figure 6. Representation of the structure of $M^{\bullet-}$, M^{2-}, $MV^{\bullet-}$, and πD^{2-} and their calculated absorption spectra. The main absorption bands have been represented as sticks and for the first one, the corresponding molecular orbitals have been provided. For $MV^{\bullet-}$ and πD^{2-}, the electronic density difference along this transition has also been represented. Increase and decrease of electron density are represented in blue and green respectively. Full Width at Half Maximum (FWHM) = 0.2 eV.

compared to their monomer counterparts $M^{\bullet-}$ and M^{2-}. Combined with the fact that K_{MV} significantly exceeds $K_{\pi D}$, the modelled concentration profile (**Figure 5d**) and the calculated wavelength for the main absorption of all anionic species (**Figure 6**), we can formulate a reasonable hypothesis to interpret the shape of the optical signature PC1 and PC2 (**Figure 5f**). PC1 is the superposition of predominantly $MV^{\bullet-}$ absorbing at 1195 nm with a weak contribution from $M^{\bullet-}$ explaining the shouldering around 1000 nm. $M^{\bullet-}$ becomes the major species in PC2, emerging from

a broad absorption of πD^{2-}. In dimers $MV^{\cdot-}$ and πD^{2-}, both monomers are involved together in the first main absorption transition as shown by the molecular orbitals and electron density difference (EDD) maps in **Figure 6**. This indicates strong intermolecular electronic communication within the $MV^{\cdot-}$ and πD^{2-} anion species.

Structure-Properties Relationship

Taken together, these experiments enable us to determine precise structure-properties relationships and explore the chemical space and possibilities offered by the *ortho*-pentannulated AzaBPDI and BACD platforms. The equilibrium constant K_{MV} and $K_{\pi D}$. are difficult to measure experimentally, but their relative values can be compared by estimating the comproportionation constant K_{com}. When monomers M are reduced, MV species $[M\text{-}M]^{\cdot-}$ are formed, in competition with neutral dimers [M-M] and π-dimer $[M\text{-}M]^{2-}$ following this equilibrium: $[M\text{-}M] + [M\text{-}M]^{2-} \rightleftharpoons [M\text{-}M]^{\cdot-} + [M\text{-}M]^{\cdot-}$. It is linked to K_{com}: the higher K_{com} is, the stronger and more stable are the MV species $[M\text{-}M]^{\cdot-}$. K_{com} can be estimated to compare MV species formed in specific experimental conditions[8] using the following equations:

$$\Delta G_{com} = -RTln(K_{com})$$

where R is the gas constant, T the temperature in K (here 293 K), and the free enthalpy of the reaction ΔG_{com} can be estimated from:

$$\Delta E = -\Delta G_{com}/F$$

where F is the Faraday constant and ΔE can be directly measured on the CV as the difference between the two maximums of the splitting event of the first reduction wave. By analysis of all CV experiments and the K_{com} values (**Figure 7a**), we can determine what are the critical structural parameters necessary to the observation of this phenomenon in this family of molecules (**Figure 7b**). For fused-AzaBPDIs, electrochemistry reveals that only **aPDI-CF$_3$** exhibits significant splitting at high concentrations, likely due to additional electronic stabilization owing to its electron-withdrawing side-group compared to the phenyl and methoxy appended analogues. This effect is lost upon dilution when equipped with short secondary imide chains but is retained in an analogue bearing long chains branched at position 2, improving lateral van der Waals interactions. Thus, fused-**aPDIs** highlight the importance of both electronic and structural effects: electronic stabilization of the radical anion and the use of imide chains improving lateral interactions and potentially reinforcing shielding from the solvent appear to be critical parameters for improving the stability of the assembly of the radical anion into intermolecular and supramolecular MV complexes. Non-fused BACDs with peripherical phenyl units also show weak splitting in CV, which persists upon dilution, indicating that extending the size of the π- system reinforces this effect. At last, the complete fusion of lateral aromatic groups to the *ortho* position in *ortho*-fused BACDs affords strong splitting in CV experiments in association to high K_{com} in the 10^3 range, reaching 10^5 for the CF_3 decorated molecules confirming the trend observed for AzaBPDIs. A regioisomerism-dependent effect is also observed, with 1,6 regioisomers displaying larger splitting and higher K_{com} than their 1,7 counterparts. Remarkably, the K_{com} measured here are in the same range as those of some binuclear metallic complexes covalently bridged by ligands.[9–11] This high sensibility of the BACD platform to small structural and electronic changes render them highly tuneable electron-deficient molecular scaffolds for the design of more elaborated materials.

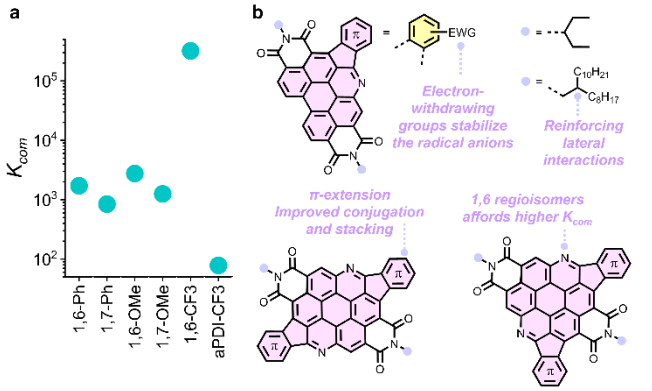

Figure 7. a) K_{com} values calculated from the ΔE measured during the CV experiments. b) Structure-properties relationship for *ortho*-pentannulated AzaBPDIs and *ortho*-pentannulated BACDs toward the formation of supramolecular anionic mixed valence species.

Conclusion

In conclusion, we have synthesized a library of *ortho*-pentannulated AzaBPDIs and BACDs. The latter are self-assembled into supramolecular polymers in chlorinated solvents as demonstrated by UV-vis absorption spectroscopy supported by molecular dynamics. From this ability to self-assemble emerges peculiar electronic properties. A strong splitting of the first reduction wave into two distinct events was observed during cyclic voltammetry experiments and attributed to the successive formation of intermolecular anionic mixed-valence and π-dimer species, as elucidated by spectroelectrochemical experiments and quantum chemistry calculations. Such observations are unprecedented for rylene diimide dyes which are not covalently linked or mechanically bonded in organic solvents. The remarkable comproportionation constants K_{com} calculated for these species are the demonstration of very stable mixed-valence species. Consequently, the driving force here is the formation of strongly associated MV complexes and not solvophobic effect as in previously reported systems. Furthermore, MV states can be selectively formed by progressive electron injection, with no co-existence with π-dimers, which is crucial to produce highly conductive supramolecular electronic materials. At last, we identified the key electronic and structural parameters required to observe the formation of these intermolecular anionic complexes and strengthen them. This original behaviour of *ortho*-pentannulated BACDs might arise from their ability to delocalize their radical anion on their large electron-deficient π surface combined to their intrinsic tendency to self-assemble by π-π interactions. The observation of intermolecular mixed-valence assemblies is of high fundamental interest, as they could be exploited in several applications. Firstly, the initial reduction leading instantaneously to the formation of the complex can be seen as the redox-triggered self-assembly of anion-π[57] dimers by interaction of a negatively charged species with an electron-deficient aromatic surface. The elaboration of structures based on anion-π interactions lately found several applications ranging

from self-assembly to sensing.[58] Secondly, we envision that *ortho*-fused BACDs are highly tuneable molecules for the elaboration of supramolecular electron-transporting materials for organic electronics. Thus, we believe that this study could advance the development of new electron-accepting materials, considering that the remarkable performances of electron-rich materials have sometimes been attributed to their ability to display such MV states. Moreover, the behaviour of *ortho*-pentannulated BACDs highlights the fact that despite the intense synthetic efforts focussed on rylene diimide dyes over the past decades, this family of electron acceptors still holds many surprises and strong potential for the discovery and assembly of new functional optoelectronic architectures.[59–61]

Acknowledgements

The authors acknowledge the Université d'Angers and SFR MATRIX. Benjamin Siegler is acknowledged for high temperature NMR experiments, along with Ingrid Freuze for mass spectrometry measurements. Arnaud Brosseau is acknowledged for discussions on spectroscopy experiments. This work received support from the "Étoiles Montantes" funding scheme (A. Goujon, project CURVY, 2021_11614, fellowship for A.H.G. David) funded by the PULSAR 2021 program from the Région Pays de la Loire and the Université d'Angers, and the Agence Nationale de la Recherche (A. Goujon, PhotoSynth ANR JCJC 2021, ANR-21-CE06-0015-01, fellowship to A. Gapin). This work received financial support under the EUR LUMOMAT project and the Investments for the Future program ANR-18E-EURE-0012 for H. Melnychenko as Master LUMOMAT student. This work is funded by the European Union (ERC Starting Grant, PhotoFreeze, project n°101116355, fellowship to M. Roger. L. L. B thanks the supercomputer facilities of the Mésocentre de calcul de Franche-Comté.

Keywords: rylene diimide • mixed valence • spectroelectrochemistry • self-assembly • organic semiconductors

References

[1] A. Jain, S. J. George, *Mater. Today* **2015**, *18*, 206–214.
[2] H. Chen, J. F. Stoddart, *Nat. Rev. Mater.* **2021**, *6*, 804–828.
[3] T. A. Barendt, M. L. Ball, Q. Xu, B. Zhang, B. Fowler, A. Schattman, V. C. Ritter, M. L. Steigerwald, C. Nuckolls, *Chem. – Eur. J.* **2020**, *26*, 3744–3748.
[4] E. Busseron, Y. Ruff, E. Moulin, N. Giuseppone, *Nanoscale* **2013**, *5*, 7098–7140.
[5] J. J. I. Armao, M. Maaloum, T. Ellis, G. Fuks, M. Rawiso, E. Moulin, N. Giuseppone, *J. Am. Chem. Soc.* **2014**, *136*, 11382–11388.
[6] J. B. Torrance, *Acc. Chem. Res.* **1979**, *12*, 79–86.
[7] S. F. Nelsen, *Chem. – Eur. J.* **2000**, *6*, 581–588.
[8] D. M. D'Alessandro, F. R. Keene, *Chem. Soc. Rev.* **2006**, *35*, 424–440.
[9] C.. Creutz, H. Taube, *J. Am. Chem. Soc.* **1973**, *95*, 1086–1094.
[10] W. Kaim, A. Klein, M. Glöckle, *Acc. Chem. Res.* **2000**, *33*, 755–763.
[11] B. S. Brunschwig, C. Creutz, N. Sutin, *Chem. Soc. Rev.* **2002**, *31*, 168–184.
[12] J. Hankache, O. S. Wenger, *Chem. Rev.* **2011**, *111*, 5138–5178.
[13] A. Heckmann, C. Lambert, *Angew. Chem. Int. Ed.* **2012**, *51*, 326–392.
[14] R. Murase, C. F. Leong, D. M. D'Alessandro, *Inorg. Chem.* **2017**, *56*, 14373–14382.
[15] J. B. Torrance, B. A. Scott, B. Welber, F. B. Kaufman, P. E. Seiden, *Phys. Rev. B* **1979**, *19*, 730–741.
[16] L. Huchet, S. Akoudad, E. Levillain, J. Roncali, A. Emge, P. Bäuerle, *J. Phys. Chem. B* **1998**, *102*, 7776–7781.
[17] M. B. Nielsen, C. Lomholt, J. Becher, *Chem. Soc. Rev.* **2000**, *29*, 153–164.
[18] M. Bendikov, F. Wudl, D. F. Perepichka, *Chem. Rev.* **2004**, *104*, 4891–4946.
[19] X. Li, J. Yang, Y.-W. Yang, *Mater. Chem. Front.* **2023**, *7*, 1463–1481.
[20] H. Spanggaard, J. Prehn, M. B. Nielsen, E. Levillain, M. Allain, J. Becher, *J. Am. Chem. Soc.* **2000**, *122*, 9486–9494.
[21] L. Đorđević, C. Valentini, N. Demitri, C. Mézière, M. Allain, M. Sallé, A. Folli, D. Murphy, S. Mañas-Valero, E. Coronado, D. Bonifazi, *Angew. Chem. Int. Ed.* **2020**, *59*, 4106–4114.
[22] N. Leblanc, N. Mercier, O. Toma, A. H. Kassiba, L. Zorina, P. Auban-Senzier, C. Pasquier, *Chem. Commun.* **2013**, *49*, 10272–10274.
[23] L. L. Miller, K. R. Mann, *Acc. Chem. Res.* **1996**, *29*, 417–423.
[24] M. Yoshizawa, K. Kumazawa, M. Fujita, *J. Am. Chem. Soc.* **2005**, *127*, 13456–13457.
[25] L. Yang, P. Langer, E. S. Davies, M. Baldoni, K. Wickham, N. A. Besley, E. Besley, N. R. Champness, *Chem. Sci.* **2019**, *10*, 3723–3732.
[26] J. C. Barnes, A. C. Fahrenbach, S. M. Dyar, M. Frasconi, M. A. Giesener, Z. Zhu, Z. Liu, K. J. Hartlieb, R. Carmieli, M. R. Wasielewski, J. F. Stoddart**,** *Proc Natl Acad Sci U S A*, **2012**, *109*, 11546–11551.
[27] Y. Jiao, H. Mao, Y. Qiu, G. Wu, H. Chen, L. Zhang, H. Han, X. Li, X. Zhao, C. Tang, X.-Y. Chen, Y. Feng, C. L. Stern, M. R. Wasielewski, J. F. Stoddart, *J. Am. Chem. Soc.* **2022**, *144*, 23168–23178.
[28] X.-J. Wang, L.-B. Xing, W.-N. Cao, X.-B. Li, B. Chen, C.-H. Tung, L.-Z. Wu, *Langmuir* **2011**, *27*, 774–781.
[29] F. Le Derf, E. Levillain, G. Trippé, A. Gorgues, M. Sallé, R.-M. Sebastían, A.-M. Caminade, J.-P. Majoral, *Angew. Chem. Int. Ed.* **2001**, *40*, 224–227.
[30] Y. Cotelle, M. Hardouin-Lerouge, S. Legoupy, O. Alévêque, E. Levillain, P. Hudhomme, *Beilstein J. Org. Chem.* **2015**, *11*, 1023–1036.
[31] V. Singh, S. Kwon, Y. Choi, S. Ahn, G. Kang, Y. Yi, M. H. Lim, J. Seo, M.-H. Baik, H. R. Byon, *Adv. Mater.* **2023**, *35*, 2210859.
[32] J.-F. Penneau, L. L. Miller, *Angew. Chem. Int. Ed. Engl.* **1991**, *30*, 986–987.
[33] J. F. Penneau, B. J. Stallman, P. H. Kasai, L. L. Miller, *Chem. Mater.* **1991**, *3*, 791–796.
[34] T. Jiao, K. Cai, J. N. Nelson, Y. Jiao, Y. Qiu, G. Wu, J. Zhou, C. Cheng, D. Shen, Y. Feng, Z. Liu, M. R. Wasielewski, J. F. Stoddart, H. Li, *J. Am. Chem. Soc.* **2019**, *141*, 16915–16922.
[35] V. Paulino, A. Mukhopadhyay, I. Tsironi, K. Liu, D. Husainy, C. Liu, K. Meier, J.-H. Olivier, *J. Phys. Chem. C* **2021**, *125*, 10526–10538.
[36] K. Liu, V. Paulino, A. Mukhopadhyay, B. Bernard, A. Kumbhar, C. Liu, J.-H. Olivier, *Phys. Chem. Chem. Phys.* **2021**, *23*, 2703–2714.
[37] M. Stępień, E. Gońka, M. Żyła, N. Sprutta, *Chem. Rev.* **2017**, *117*, 3479–3716.
[38] A. Borissov, Y. K. Maurya, L. Moshniaha, W.-S. Wong, M. Żyła-Karwowska, M. Stępień, *Chem. Rev.* **2022**, *122*, 565–788.
[39] A. Goujon, L. Rocard, T. Cauchy, P. Hudhomme, *J. Org. Chem.* **2020**, *85*, 7218–7224.
[40] H. Zhylitskaya, M. Stępień, *Org. Chem. Front.* **2018**, *5*, 2395–2414.
[41] W. Hagui, H. Doucet, J.-F. Soulé, *Chem* **2019**, *5*, 2006–2078.
[42] A. Gapin, A. H. G. David, M. Allain, D. Masson, O. Alévêque, T. Ave, L. Le Bras, P. Hudhomme, A. Goujon, *Chem. – Eur. J.* **2023**, *29*, e202300652.
[43] While writing this research article, Wu, Xia and co-workers reported a similar ortho-pentannulated AzaBPDI possessing long branched alkyls chains albeit with lower yields for the Pd-catalyzed intramolecular C−H arylation. The authors employed this compound for building organic field-effect transistors. F. Yang, C. Wang, L. Liang, Z. Wang, X. You, G. Shao, D. Wu, J. Xia, *Chem. Eur. J.* **2024**, e202401074.
[44] D. Schmidt, M. Son, J. M. Lim, M.-J. Lin, I. Krummenacher, H. Braunschweig, D. Kim, F. Würthner, *Angew. Chem. Int. Ed.* **2015**, *54*, 13980–13984.
[45] A. Nowak-Król, K. Shoyama, M. Stolte, F. Würthner, *Chem. Commun.* **2018**, *54*, 13763–13772.

[46] I. Tabakovic, L. L. Miller, R. G. Duan, D. C. Tully, D. A. Tomalia, *Chem. Mater.* **1997**, *9*, 736–745.
[47] S. T. Schneebeli, M. Frasconi, Z. Liu, Y. Wu, D. M. Gardner, N. L. Strutt, C. Cheng, R. Carmieli, M. R. Wasielewski, J. F. Stoddart, *Angew. Chem. Int. Ed.* **2013**, *52*, 13100–13104.
[48] Y. Wu, M. Frasconi, D. M. Gardner, P. R. McGonigal, S. T. Schneebeli, M. R. Wasielewski, J. F. Stoddart, *Angew. Chem. Int. Ed.* **2014**, *53*, 9476–9481.
[49] F. Schlosser, M. Moos, C. Lambert, F. Würthner, *Adv. Mater.* **2013**, *25*, 410–414.
[50] S. E. Penty, M. A. Zwijnenburg, G. R. F. Orton, P. Stachelek, R. Pal, Y. Xie, S. L. Griffin, T. A. Barendt, *J. Am. Chem. Soc.* **2022**, *144*, 12290–12298.
[51] A. Takai, T. Yasuda, T. Ishizuka, T. Kojima, M. Takeuchi, *Angew. Chem. Int. Ed.* **2013**, *52*, 9167–9171.
[52] O. Alévêque, C. Gautier, E. Levillain, *Curr. Opin. Electrochem.* **2019**, *15*, 34–41.
[53] O. Alévêque, E. Levillain, L. Sanguinet, *Electrochem. Commun.* **2015**, *51*, 108–112.
[54] F. Gaillard, E. Levillain, *J. Electroanal. Chem.* **1995**, *398*, 77–87.
[55] C. Amatore, O. Klymenko, I. Svir, *Electrochem. Commun.* **2010**, *12*, 1165–1169.
[56] M. J. Frisch, G. W. Trucks, H. B. Schlegel, G. E. Scuseria, M. A. Robb, J. R. Cheeseman, G. Scalmani, V. Barone, G. A. Petersson, H. Nakatsuji, X. Li, M. Caricato, A. Marenich, J. Bloino, B. G. Janesko, R. Gomperts, B. Mennucci, H. P. Hratchian, J. V. Ortiz, A. F. Izmaylov, J. L. Sonnenberg, D. Williams-Young, F. Ding, F. Lipparini, F. Egidi, J. Goings, B. Peng, A. Petrone, T. Henderson, D. Ranasinghe, V. G. Zakrzewski, J. Gao, N. Rega, G. Zheng, W. Liang, M. Hada, M. Ehara, K. Toyota, R. Fukuda, J. Hasegawa, M. Ishida, T. Nakajima, Y. Honda, O. Kitao, H. Nakai, T. Vreven, K. Throssell, J. A. Montgomery, Jr., J. E. Peralta, F. Ogliaro, M. Bearpark, J. J. Heyd, E. Brothers, K. N. Kudin, V. N. Staroverov, T. Keith, R. Kobayashi, J. Normand, K. Raghavachari, A. Rendell, J. C. Burant, S. S. Iyengar, J. Tomasi, M. Cossi, J. M. Millam, M. Klene, C. Adamo, R. Cammi, J. W. Ochterski, R. L. Martin, K. Morokuma, O. Farkas, J. B. Foresman, D. J. Fox, *Gaussian 09, Revision C.01*, Gaussian, Inc., Wallingford CT, 2016.
[57] R. E. Dawson, A. Hennig, D. P. Weimann, D. Emery, V. Ravikumar, J. Montenegro, T. Takeuchi, S. Gabutti, M. Mayor, J. Mareda, C. A. Schalley, S. Matile, *Nat. Chem.* **2010**, *2*, 533–538.
[58] B. L. Schottel, H. T. Chifotides, K. R. Dunbar, *Chem. Soc. Rev.* **2007**, *37*, 68–83.
[59] A. Nowak-Król, F. Würthner, *Org. Chem. Front.* **2019**, *6*, 1272–1318.
[60] F. Würthner, C. R. Saha-Möller, B. Fimmel, S. Ogi, P. Leowanawat, D. Schmidt, *Chem. Rev.* **2016**, *116*, 962–1052.
[61] R. K. Dubey, F. Würthner, *Nat. Chem.* **2023**, *15*, 884–884.

The authors have cited additional references within the Supporting Information.

[62] A. H. G. David, D. Shymon, H. Melville, L.-A. Accou, A. Gapin, M. Allain, O. Alévêque, M. Force, A. Grosjean, P. Hudhomme, L. L. Bras, A. Goujon, *J. Mater. Chem. C* **2023**, *11*, 14631–14640.
[63] Z. Chen, A. Lohr, C. R. Saha-Möller, F. Würthner, *Chem. Soc. Rev.* **2009**, *38*, 564–584.
[64] R. B. Martin, *Chem. Rev.* **1996**, *96*, 3043–3064.
[65] M. J. Abraham, T. Murtola, R. Schulz, S. Páll, J. C. Smith, B. Hess, E. Lindahl, *SoftwareX* **2015**, *1–2*, 19–25.
[66] J. Wang, R. M. Wolf, J. W. Caldwell, P. A. Kollman, D. A. Case, *J. Comput. Chem.* **2004**, *25*, 1157–1174.
[67] J. Wang, W. Wang, P. A. Kollman, D. A. Case, *J. Mol. Graph. Model.* **2006**, *25*, 247–260.
[68] P. R. Batista, A. Wilter, E. H. A. B. Durham, P. G. Pascutti, *Cell Biochem. Biophys.* **2006**, *44*, 395–404.
[69] T. Darden, D. York, L. Pedersen, *J. Chem. Phys.* **1993**, *98*, 10089–10092.
[70] H. J. C. Berendsen, J. P. M. Postma, W. F. van Gunsteren, A. DiNola, J. R. Haak, *J. Chem. Phys.* **1984**, *81*, 3684–3690.
[71] U. Essmann, L. Perera, M. L. Berkowitz, T. Darden, H. Lee, L. G. Pedersen, *J. Chem. Phys.* **1995**, *103*, 8577–8593.
[72] S. Nosé, M. L. Klein, *Mol. Phys.* **1983**, *50*, 1055–1076.
[73] S. Nosé, *J. Chem. Phys.* **1984**, *81*, 511–519.
[74] W. G. Hoover, *Phys. Rev. A* **1985**, *31*, 1695–1697.
[75] M. Parrinello, A. Rahman, *J. Appl. Phys.* **1981**, *52*, 7182–7190.
[76] J. Tomasi, B. Mennucci, R. Cammi, *Chem. Rev.* **2005**, *105*, 2999–3094.

Table of Contents

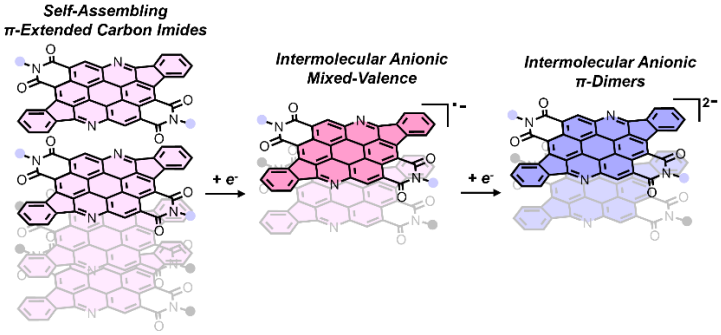

We report the serendipitous discovery of intermolecular anionic mixed-valence and π-dimer species in *ortho*-pentannulated BisAzaCoroneneDiimides during their electrochemical reduction in a non-aqueous solvent. The observation of this phenomenon provides insights into the fundamental behaviour of supramolecular organic semiconductors, thereby paving the way for the development of novel electronic devices and electron-deficient materials.